

# On the Piecewise Parabolic Method for Compressible Flow with Stellar Equations of State

Michael Zingale and Max P. Katz

*Dept. of Physics and Astronomy, Stony Brook University, Stony Brook, NY 11794-3800*

Michael.Zingale@stonybrook.edu

## ABSTRACT

The piecewise parabolic method and related schemes are widely used to model stellar flows. Several different methods for extending the validity of these methods to a general equation of state have been proposed over time, but direct comparisons amongst one-another and exact solutions with stellar equations of state are not widely available. We introduce some simple test problems with exact solutions run with a popular stellar equation of state and test how two existing codes with different approaches to incorporating general gases perform. The source code for generating the exact solutions is made available.

## 1. Introduction

Many stellar flows are modeled with compressible hydrodynamics methods, with the piecewise parabolic method (PPM) (Colella & Woodward 1984) being one of the most popular algorithms. All extant astrophysical hydrodynamics codes that include a general equation of state augment the PPM algorithm with additional information about the energy of the fluid and use Riemann solvers designed to approximate the wave structure of the solution without requiring expensive equation of state calls. However, little attention in the literature has been given to verifying these simulation codes directly for the degenerate stellar equation of state. While plenty of shock-tube Riemann problems exist for a simple gamma-law gas (e.g. Sod 1978), these do not test the algorithms when the gamma of the gas changes dramatically in the problem. We introduce some shock tube problems for the general stellar equation of state and compare the hydrodynamic solution to the exact solution of the Riemann problem for these tests. Different codes make different choices when dealing with a general equation of state, but no comparisons and little verification has been done on these implementations. The basic verification of these methods for stellar flows is the goal of this paper.

An important diagnostic quantity is the temperature of the gas in the star. Degenerate gases are weakly sensitive to temperature—this creates interesting challenges for hydrodynamics methods. Traditionally, pressure, not temperature, plays a central role in the construction of the fluxes through the interfaces in Godunov schemes for compressible hydrodynamics. In the piecewise parabolic method (PPM) implementation (Colella & Woodward 1984), the primitive variables,  $\rho, u, p$  are reconstructed as parabolas in each zone and we then trace under these profiles to find the information that can reach the interface over the timestep. Any small errors in the thermodynamic consistency of the interface state, introduced from the extrapolation and limiting procedures used in these methods, can lead to a large error in the temperature calculated from the equation of state for a degenerate gas. While not needed in pure hydrodynamic flows, temperature is an essential quantity for reacting flows and radiation hydrodynamics. For this reason, we look at the performance of the different methods in preventing artificial undershoots and overshoots in temperature.

In the tests below, we use the publicly-available CASTRO code (Almgren et al. 2010) as our reference and implement the variations as options in CASTRO. We also compare to the original dimensionally-split PPM solver in FLASH (Fryxell et al. 2000), that in turn was based on the PPM implementation in Fryxell et al. (1989). While we note that FLASH has other solvers available, this is the default solver in FLASH 4.0. These codes use slightly different implementations of PPM, based on original method as described by Colella & Woodward (1984) (henceforth CW) and the description in Miller & Colella (2002) (henceforth MC). They also take different approaches to the extension of the algorithm to a general equation of state. Finally, we note a small correction to the scheme used in FLASH, in Appendix A.3.

## 2. PPM Overview

The conservative Euler equations appear, in one dimension, as:

$$\frac{\partial \rho}{\partial t} + \frac{\partial(\rho u)}{\partial x} = 0 \tag{1a}$$

$$\frac{\partial(\rho u)}{\partial t} + \frac{\partial(\rho u^2)}{\partial x} + \frac{\partial p}{\partial x} = 0 \tag{1b}$$

$$\frac{\partial(\rho E)}{\partial t} + \frac{\partial(\rho u E + u p)}{\partial x} = 0 \tag{1c}$$

where  $\rho$  is the density,  $u$  is the velocity,  $p$  is the pressure, and  $E$  is the total specific energy. The equations are closed via an equation of state,

$$p = p(\rho, e) \tag{2}$$

where  $e$  is the specific internal energy,  $e = E - \frac{1}{2}u^2$ . For many astrophysical equations of state, temperature ( $T$ ), not energy, is an independent variable, and we have

$$p = p(\rho, T), \quad e = e(\rho, T) \quad (3)$$

and iterations (usually via the Newton-Raphson method) are done to find the  $T$  that gives the desired  $e$ , allowing us to then find  $p$ .

The hydrodynamics equations in terms of the standard set of primitive variables,  $\rho, u, p$ , are:

$$\frac{\partial \rho}{\partial t} + u \frac{\partial \rho}{\partial x} + \rho \frac{\partial u}{\partial x} = 0 \quad (4a)$$

$$\frac{\partial u}{\partial t} + u \frac{\partial u}{\partial x} + \frac{1}{\rho} \frac{\partial p}{\partial x} = 0 \quad (4b)$$

$$\frac{\partial p}{\partial t} + u \frac{\partial p}{\partial x} + \rho c^2 \frac{\partial u}{\partial x} = 0 \quad (4c)$$

where  $c$  is the speed of sound defined in terms of the adiabatic index  $\Gamma_1 = \partial(\log p)/\partial(\log \rho)|_s$  as

$$c^2 = \Gamma_1 p / \rho \quad (5)$$

As most papers deal with a constant- $\gamma$  ideal gas equation of state, it is important to note that the pressure equation above is completely general, and can be derived by writing  $p = p(\rho, s)$ , and differentiating along streamlines with no entropy sources. No assumptions about the constancy of  $\gamma$  are needed.

For a general EOS, we need to augment our system with additional thermodynamic information for the Riemann solver. CASTRO adds the evolution of  $(\rho e)$  to the system:

$$\frac{\partial(\rho e)}{\partial t} + u \frac{\partial(\rho e)}{\partial x} + \rho h \frac{\partial u}{\partial x} = 0 \quad (6)$$

where  $h = e + p/\rho$  is the specific enthalpy. Alternately, Colella & Glaz (1985) (henceforth CG) define  $\gamma_e = p/(\rho e) + 1$  and derive an evolution equation for it. Differentiating, we find:

$$\begin{aligned} \frac{D\gamma_e}{Dt} &= \frac{D}{Dt} \left( \frac{p}{\rho e} + 1 \right) = -\frac{p}{(\rho e)^2} \frac{D(\rho e)}{Dt} + \frac{1}{\rho e} \frac{Dp}{Dt} \\ &= (\gamma_e - 1)(\gamma_e - \Gamma_1) \frac{\partial u}{\partial x} \end{aligned} \quad (7)$$

where we used Eqs. (4c, 5, 6) to simplify. If we eliminate  $\partial u/\partial x$  in favor of  $Dp/Dt$  using Eq. 4c, then we arrive at the expression from CG. We see that for an ideal gas, since  $\gamma = \Gamma_1$ , we have  $D\gamma/Dt = 0$ .

An analysis of this system (see any standard hydrodynamics text, e.g. Toro 1997), including one of the energy equations, shows that there are three characteristic waves that carry jumps in the variables at the speeds:  $\lambda^{(-)} = u - c$ ,  $\lambda^{(o)} = u$ , and  $\lambda^{(+)} = u + c$  (with the addition of the  $(\rho e)$  or  $\gamma_e$  equation, the  $u$  eigenvalue becomes degenerate). We will use these superscripts,  $(-)$ ,  $(o)$ , and  $(+)$ , to distinguish between the waves in the following discussion.

The PPM algorithm advances the solution through a timestep using a finite-volume framework. In each zone, the average value of the state is changed by constructing the fluxes through the interfaces of the zones. The update appears as:

1. Construct limited parabolic profiles of the primitive variables,  $q_i$ , in zone  $i$  using the procedure from CW. This results in a limited parabola,  $q(x)$ . We note that alternate limiters exist (Colella & Sekora 2008) and are implemented in CASTRO, but we do not consider those here.
2. Integrate under each parabola to find the average state that can be carried to each interface by each of the characteristic waves. We define an integral  $\mathcal{I}_{\pm}^{(\nu)}(q_i)$  which is the average of the parabola profile of  $q_i$  to the left ( $-$  subscript) or right ( $+$  subscript) of the cell for the region swept out the wave ( $\nu$ ) (see Figure 1). These integrals are:

$$\mathcal{I}_{+}^{(\nu)}(q_i) = \frac{1}{\sigma^{(\nu)}\Delta x} \int_{x_{i+1/2}-\sigma^{(\nu)}\Delta x}^{x_{i+1/2}} q(x)dx \quad (8a)$$

$$\mathcal{I}_{-}^{(\nu)}(q_i) = \frac{1}{\sigma^{(\nu)}\Delta x} \int_{x_{i-1/2}}^{x_{i-1/2}+\sigma^{(\nu)}\Delta x} q(x)dx \quad (8b)$$

with  $\sigma^{(\nu)} = |\lambda^{(\nu)}|\Delta t/\Delta x$  (see MC for a discussion and motivation).

3. Perform characteristic tracing to build the interface states. Following CW and MC, the data in zone  $i$  can be used to build the states on the right interface,  $q_{i+1/2,L}^{n+1/2}$ , and on the left interface,  $q_{i-1/2,R}^{n+1/2}$ , of zone  $i$  (see Figure 2 for an illustration of the location of each of these states). These appear as:

$$q_{i+1/2,L}^{n+1/2} = \tilde{q}_{+} - \sum_{\nu;\lambda^{(\nu)}\geq 0} l_i^{(\nu)} \cdot \left( \tilde{q}_{+} - \mathcal{I}_{+}^{(\nu)}(q_i) \right) r_i^{(\nu)} \quad (9a)$$

$$q_{i-1/2,R}^{n+1/2} = \tilde{q}_{-} - \sum_{\nu;\lambda^{(\nu)}\leq 0} l_i^{(\nu)} \cdot \left( \tilde{q}_{-} - \mathcal{I}_{-}^{(\nu)}(q_i) \right) r_i^{(\nu)} \quad (9b)$$

This shows that the same set of eigenvectors and eigenvalues are used for these two states.

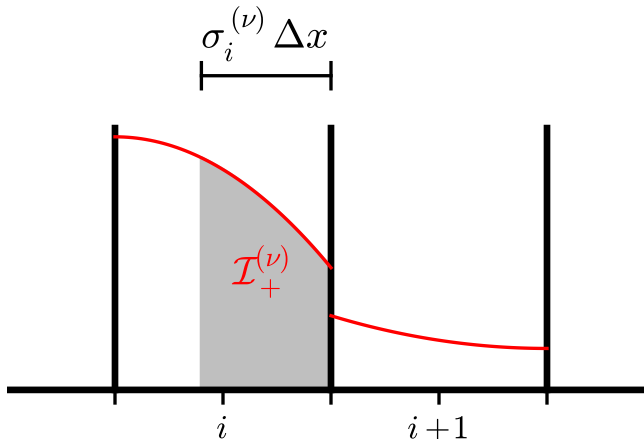


Fig. 1.— Tracing under the parabolic profile to construct  $\mathcal{I}_+^{(\nu)}(q)$  at the  $i + 1/2$  interface.

Here,  $\tilde{q}_+$  and  $\tilde{q}_-$  are the reference states, designed to minimize the amount of work done by the characteristic tracing (see the discussion in MC). The key part of this step is that the sum (Eqs. 9a and 9b) only includes the contributions for waves that are moving toward the interface. If all waves were included, then this would be a no-op (although, see the discussion in Stone et al. 2008 for HLL-type solvers).

There is a choice in the primitive variable system one can use, and therefore, the resulting left and right eigenvectors:  $l_i^{(\nu)}$  and  $r_i^{(\nu)}$ . This comes into play with a general gas since FLASH and CASTRO use a different “energy” variable in the eigensystem. Appendix A discusses the options and gives the form of the eigenvectors, and writes the states  $q_{i+1/2,\{L,R\}}^{n+1/2}$  for each variables in a notation similar to that in CW.

4. Solve the Riemann problem to find the fluxes through each interface and convert the unique interface states back to the conserved variables. There are several different Riemann solvers used for non-ideal gases in the literature. We discuss some of the options later.
5. Update the conservative variables using these fluxes.

As a side note, we remark that much of the PPM method (in one-dimension) is done to third order, but the conversion from conservative to primitive variables is only second-order accurate, and this conversion itself can introduce some thermodynamic inconsistency. McCorquodale & Colella (2011) discuss how to derive a 4th-order accurate method. Finally, we note that Colella (1990) and MC described the extension to multiple dimensions.

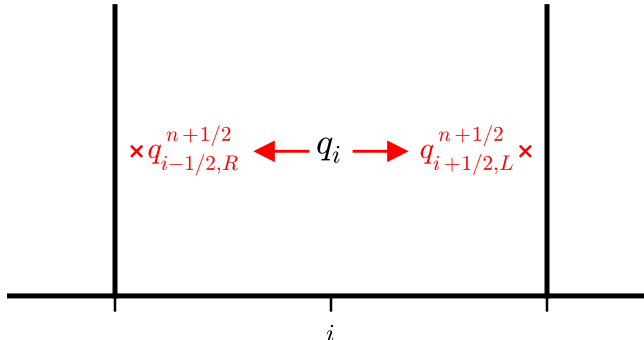


Fig. 2.— The two interfaces states constructed from the data in zone  $i$ .

## 2.1. Variations Among PPM Implementations

CASTRO was originally written to closely follow the PPM method as described in MC, which differs from the original PPM implementation (CW), and the original dimensionally-split PPM solver implemented in FLASH in several ways. Since the original paper (Almgren et al. 2010), a number of small changes were introduced, which are summarized here.

- CASTRO originally set the reference state,  $\tilde{q}_{\pm}$ , to be the cell-center value. It has been updated to use the prescription from CW, which uses the integral under the parabola for the fastest wave (if the wave moves toward the interface) or the limit of the parabolic interpolant if the wave is not moving toward the interface. These options are controlled in CASTRO through the `castro.ppm_reference` and `castro.ppm_reference_edge_limit` runtime parameters.
- In the characteristic projection, CW use  $\tau \equiv 1/\rho$  instead of  $\rho$  in the eigensystem (see the form of  $\beta^0$  in CW Eq. 3.7). MC use  $\rho$ . This is discussed in Appendix A.2, and explored in more detail later. Note however that CW do the parabolic reconstruction of  $\rho$ , not  $\tau$ . This choice is controlled in CASTRO by the parameter `castro.ppm_tau_in_tracing`.
- In the characteristic tracing, numerous terms appear of the form  $\beta \equiv (l \cdot \Delta q)$ , where  $\Delta q$  is some jump in the primitive variable  $q$ . CW evaluate these  $\beta$ 's and any other quantities in the interface state construction using the reference state (this is equivalent to evaluating the eigenvectors with the reference state). MC do not explicitly write out the expansion of the dot product and leave things in terms of eigenvectors which are constructed using the time-level  $n$  data. We use the CW method here in CASTRO, which can be selected through the `castro.ppm_reference_eigenvectors`.

- All variants described above use flattening to prevent shocks from becoming too thin, but there is variation in *when* this flattening procedure should be applied. In MC, the edge states  $q_l$  and  $q_r$  are constructed, then the PPM monotoneization procedure is applied, and finally the flattening is done to each parabola. In the FLASH split PPM solver, the flattening is done on the  $q_l$  and  $q_r$  *before* the PPM monotoneization. CW do not seem to indicate which of these orderings is preferred. Both of these do the flattening before the parabolas are integrated. We note that the flattening function in CW is written in a different form than in MC, but they are analytically equivalent. CASTRO by default applies the flattening after the integrals  $\mathcal{I}$  are constructed from the parabola, when constructing the final edge states. These differences do not seem to influence the solution much. The different methods can be explored in CASTRO through the parameter `castro.ppm.flatten.before.integrals`. We note that not all PPM implementations use flattening—by default ENZO (Bryan et al. 2014) has it disabled. In the tests that follow, we adopt the FLASH ordering of flattening and then limiting in CASTRO.

Finally, CW use a contact steepening algorithm to keep contact discontinuities thin. MC and CASTRO do not implement this, but the FLASH split PPM solver does and uses it by default. For the FLASH runs presented here, we disable contact steepening. Some authors (e.g. Stone et al. 2008) suggest limiting on the characteristic variables themselves. This is the default in the latest version of the FLASH dimensionally-split PPM solver, and we will look at its influence when we compare with FLASH.

## 2.2. Extension to a General EOS

CW do not address how to extend PPM to a general equation of state. Most works cite CG as the inspiration for dealing with a general EOS, in particular, for the Riemann problem, but other variations exist. CG predict an interface value of  $\gamma_e \equiv p/(\rho e) + 1$  using an equation that captures the thermodynamic evolution along streamlines (similar to Eq. 7). We note that CG did not discuss how to use parabolic reconstruction of the fluid quantities with a general EOS. Their  $\gamma_e$  does not participate in the characteristic tracing described above; rather, it is constructed from the predicted interface value of  $p$ , using the average  $\Gamma_1$  and  $\gamma_e$  on either side of the interface. Since  $\Gamma_1$  does not explicitly appear in the fluxes, CG argue that taking the cell-average value for the interface is second-order accurate.

The FLASH dimensionally-split PPM solver reconstructs  $\gamma_e$  and  $\Gamma_1$  as parabolas and integrates under the  $\lambda^{(o)}$  wave to get their interface values (note: this does not appear to be documented in the FLASH paper). This differs substantially from CG, and suggests that they

both should obey a hyperbolic PDE. We show in Appendix A.3 that it is possible to include  $\gamma_e$  in the characteristic projection and it can actually jump across all three characteristic waves, not just the  $\lambda^{(o)}$  wave as assumed in FLASH. We know of no method to allow for a high-order reconstruction of  $\Gamma_1$  to the interface. In the construction of the interface states, FLASH evaluates the Lagrangian sound speed,  $C$ , using  $\tilde{p}$ ,  $\tilde{\rho}$ , but with the cell-centered  $\Gamma_1$ . This is correct if we choose not to predict  $\Gamma_1$  to the interfaces using parabolic reconstruction, but potentially inconsistent with a general EOS if you do. In CW,  $\Gamma_1 = \gamma_e = \gamma$  was constant, so the issue of what  $\Gamma_1$  to use in  $\tilde{C}$  was not discussed.

CASTRO includes an evolution equation for  $(\rho e)$ , which appears as an additional hyperbolic PDE in the primitive variable system. This is reconstructed and enters into the characteristic tracing in the same fashion as all the other primitive variables (see Appendix A.1).

Solving the Riemann problem exactly for a general equation of state is expensive (see Appendix B). Both the FLASH dimensionally-split PPM solver and CASTRO use an approximate two-shock Riemann solver. Here, the left and right waves are assumed to be shocks and jump conditions are used to link to the state in-between these waves. This middle state is traditionally called the “star”-region. To describe the thermodynamics of our general gas, auxiliary information is needed to supplement the primitive variables. CG use the same evolution equation that predicted the interface value of  $\gamma_e$  to predict the value of  $\gamma_e$  in the star-region of the Riemann problem. This is an iterative method that converges to find a value of the nonlinear wavespeeds across the (presumed) shocks in the Riemann problem. This is then used to construct the energy in the star-region. FLASH uses the parabolically-traced values of  $\gamma_e$  as input to the CG Riemann solver.

CASTRO instead uses the interface values of  $(\rho e)$  along with  $\rho$ ,  $u$ , and  $p$  as input to the Riemann problem. The default solver in CASTRO follows the procedure in (Colella et al. 1997; Bell et al. 1989) where jump conditions are used to estimate a value of  $(\rho e)$  in the star region. However the option exists to use the CG Riemann solver with interface values of  $\gamma_e$  set as:

$$\gamma_{e_s} = \frac{p_s}{(\rho e)_s} + 1 \quad (10)$$

where  $p_s$  and  $(\rho e)_s$  are the predicted interface values of  $p$  and  $(\rho e)$ , and  $s \in \{l, r\}$  indicates whether we are to the left or right of the interface.

There are other potential choices for Riemann solvers. The HLL solvers (Harten et al. 1983; Einfeldt 1988) use the jump conditions and simple estimates of the wave speeds to give the fluxes directly, and should work for a general gas without issue. The HLLC solver advocated by Toro (Toro 1997) would need modification for a general gas because of the construction of the speed of the contact wave.



Each of these methods incorporates information about  $e$  in some fashion. We note that there is a potential for thermodynamic inconsistency on the interfaces—the quantities  $\rho$ ,  $p$ , and  $\gamma_e$  or  $(\rho e)$  were brought to the interfaces independent of one another, subjected to limiting, flattening, and characteristic tracing. In fact, they are not independent, and there is an error in how well these interface states obey the equation of state.

### 3. Numerical Tests

Little, if any, comparison of astrophysical hydrodynamics codes to exact solutions of the shock tube problem has been done. Generating exact solutions for an arbitrary equation of state is straightforward—these are the exact solutions to the Riemann problem. Colella & Glaz (1985) outline the procedure to exactly solve the Riemann problem. In Appendix B we summarize some of the implementation details and give the initial conditions for four problems: a Sod-like problem, a double rarefaction, a strong shock, and conditions mimicking the edge of an under-resolved star. The first three are our stellar EOS analogs to the standard test problems from Toro (1997). The tests presented here are not exhaustive, but sample some of the flow conditions we might encounter in large-scale simulations. We note that  $\gamma_e$  is not constant in these tests—and in test 4, it varies through its entire valid range.

We use CASTRO as the main code to test our ideas, but we also run the same tests “as-is” with the FLASH dimensionally-split PPM solver (Fryxell et al. 2000) (version 4.0) just for comparison. This solver in FLASH can be thought of as the CW method, performing a reconstruction of both  $\gamma_e$  and  $\Gamma_1$ . In the discussion below, we use “FLASH” to mean this specific dimensionally-split PPM solver.

CASTRO is primarily a 2- and 3-D code, so we do all the runs in 2-D, with the transverse direction simply replicating the shock tube problem. This means that the transverse flux difference will have no contribution to the interface states. For all CASTRO tests, we use the iterative Riemann solver described in Colella & Glaz (1985) (this is enabled with the CASTRO option `castro.use_colglaz=1`) unless otherwise specified.

The main driver in FLASH is written with dimensional splitting in mind, so the PPM solver takes a cycle consisting of two timesteps with equal  $\Delta t$  (swapping the ordering of the directional sweeps in multiple dimensions) and then re-evaluates  $\Delta t$  based on the flow conditions in the domain. We run FLASH in 1-D, and to have the timestepping match CASTRO, we allow FLASH to only take a single timestep per cycle. Both codes will modify the last timestep to end at the time defined by the problem. This change to the timestepping

is the only change we made to FLASH.

We note that some variation of these results can be expected with varying CFL number or using an initially small timestep, but we will not explore these details. All runs use 128 zones, a CFL number of 0.8, and take an initial timestep of 0.1 of the CFL step. We also restrict the maximum increase in  $\Delta t$  from one step to the next to be 10%.

Both codes use the same full stellar equation of state described in Timmes & Swesty (2000); Fryxell et al. (2000). A low temperature floor,  $T_{\text{small}} = 10^4$  K, is imposed by the equation of state. It is important to note how this small temperature floor is applied. During the hydrodynamics solve, we typically enter the EOS with  $\rho, e_{\text{want}}, X_k$  and ask for  $p, T$ . The equation of state most naturally deals with  $\rho, T, X_k$  as inputs, so we must do a Newton-Raphson iteration to get the energy,  $e_{\text{want}}$  we want. During the iteration, if  $T < T_{\text{small}}$ , then we stop our iteration and return the thermodynamic state corresponding to the temperature floor. The problem is that  $e_{\text{small}} = e(\rho, T_{\text{small}}, X_k) \neq e_{\text{want}}$ , so we either break energy conservation by resetting the hydrodynamic state to  $e_{\text{small}}$  or break thermodynamic consistency by keeping  $e_{\text{want}}$ . For the simulations presented here, we found that keeping the thermodynamic consistency is more important to getting a good temperature field, and this is the procedure used in both codes (this is the default behavior in FLASH and controlled by the `eos_input_is_constant` parameter in the `&extern` namelist in CASTRO).

### 3.1. Comparison of Riemann Solvers

Our first comparison is to look at the difference in the solution between the CG Riemann solver and the solver presented in Colella et al. (1997) (henceforth called CGF), which was the default Riemann solver used in Almgren et al. (2010). We focus on tests 1 and 4, since those are the only tests that show substantial differences. Figure 3 shows the density, velocity, pressure, and temperature fields for the two cases together with the exact solution. Figure 4 shows the error against the exact solution for these two runs. The temperature field shows the most differences (amongst the two solvers and against the exact solution). We see an oscillation in the CGF temperature solution behind the contact discontinuity and a slightly more pronounced undershoot in the temperature in the CG solver. Both are unphysical. Looking at the density and pressure errors, we see slightly larger error between the contact and rarefaction in the CGF case than in the CG case. Figure 5 shows the comparison for test 4. Here we see differences in the velocity on the right of the domain and differences in achieving the cool temperature behind the rarefaction. The CGF gets closer to the temperature minimum. Going forward, we use the CG solver exclusively to avoid the oscillations seen in test 1, but these results leave the door open to exploring other Riemann

solvers for general equations of state.

### 3.2. Using $\rho$ vs. $\tau$ in the Characteristic Tracing

Here we examine the effect of using  $\tau = 1/\rho$  instead of  $\rho$  in defining the eigensystem used for the characteristic tracing. In essence we are comparing the original CW method to CASTRO’s implementation of the MC method. Again, only test 1 shows any difference, and again it is slight. Figure 6 shows the temperature results for test 1. The difference here is so slight that it seems that this variation does not really matter.

### 3.3. Comparisons with FLASH

Finally we summarize by comparing CASTRO’s method to FLASH. In some sense, this allows us to investigate the differences between using  $\gamma_e$  vs.  $\rho e$  in the interface states (although, see Appendix A.3). We use both the default options in FLASH (characteristic limiting) and a run with the characteristic limiting disabled. Figures 7 through 10 show the results. In test 1, the CASTRO solution appears to suffer the least amount of temperature undershoot behind the contact, with the FLASH solution without limiting on the characteristic variables also looking good, and the default FLASH having the deepest undershoot. This suggests that the characteristic limiting may not always be a good idea, and its use should depend on what quantities you are looking to optimize. For tests 2 and 3, there do not seem to be any major differences—all solvers show the same features. For test 4, all of the methods have difficulty resolving the narrow region between the rarefaction and the contact, and largely look the same, except for the velocity, where all the methods have trouble finding the correct velocity at the right edge of the domain.

## 4. Discussion

While the basic PPM algorithm is now 30 years old, there are a large number of variations in the literature. We looked at the implementations in CASTRO and FLASH, and performed verification tests on whether they can accurately model stellar flows. The main, simple message of this paper is that it is possible to do verification of stellar hydrodynamics codes on problems with a real stellar equation of state, and of course, that one should be in the habit of doing this. Part of the inspiration for this exploration was the common appearance of temperature “funniness” such as flooring or oscillations (see, e.g. the comparisons

in Almgren et al. 2006) in hydrodynamic flows. These tests can be used to help design new methods that optimize for a particular behavior.

Our tests showed that the different approaches that FLASH and CASTRO take toward incorporating the real equation of state into the solution appear reasonable and consistent with one another. They also showed that the updates to CASTRO highlighted in § 2.1 perform well. In developing the structure of the eigensystem when  $\gamma_e$  was added, we made a recommendation for the FLASH dimensionally-split PPM solver to improve the prediction of  $\gamma_e$  to the interfaces. We stress that the tests here are not complete and much more exploration can be done.

The multidimensional treatment of these methods, and dealing with a general equation of state, is more complex. In an unsplit method (e.g. Colella 1990) the interface states are first predicted in primitive variable form as if the system were one-dimensional, then converted back to conservative form where a transverse flux difference is added. This makes the interface states “see” what is happening in the transverse directions. Finally, the states are converted back to primitive form for the Riemann solve. This conversion can affect thermodynamic consistency, especially if it is done without involving the EOS. We note that with either  $(\rho e)$  or  $\gamma_e$  as an auxiliary variable, a transverse term will need to be incorporated. This is done in CASTRO currently, and an equation of state call can be avoided by using the multidimensional pressure equation throughout the procedure, but a detailed exploration of alternatives may still be illuminating.

Finally we suggest that future stellar hydrodynamics codes test against the exact solution to the shock tube problem for the stellar equation of state. We make our exact Riemann solver and all of the CASTRO improvements tested here freely available in the CASTRO code distribution (the Castro `Sod_stellar/` problem has all the necessary inputs). Similar test problems can be designed for the nuclear equation of state used in core-collapse supernovae simulations, although we note that the solution procedure from Colella & Glaz (1985) we follow does not work for a non-convex equation of state, so modifications will be necessary for a general nuclear equation of state.

This research was supported by NSF award AST-1211563. We thank Ann Almgren, John Bell, Alan Calder, Sean Couch, and Dongwook Lee for very helpful discussions and feedback.

## A. Eigenvectors and the Characteristic Projection

Here we summarize the eigensystems corresponding to different sets of primitive variables. We will write the interface state generically as:

$$q_s = \tilde{q}_s - \sum_{\nu} (l^{(\nu)} \cdot \Delta q_s^{(\nu)}) r^{(\nu)} \quad (\text{A1})$$

where  $s$  refers to the left or right state at an interface and the sum includes only those waves moving toward that interface. We introduce the shorthand for a jump:

$$\Delta q_s^{(\nu)} \equiv \tilde{q}_s - \mathcal{I}_s^{(\nu)}(q) \quad (\text{A2})$$

### A.1. Standard primitive variables

The standard set of primitive variables used in CASTRO for the characteristic tracing and prediction of the interface states are  $q = (\rho, u, p, \rho e)^\top$ . This evolution is governed by Eqs. 4a to 4c and 6. Written in the form

$$q_t + A(q)q_x = 0 \quad (\text{A3})$$

the matrix  $A$  takes the form

$$A(q) = \begin{pmatrix} u & \rho & 0 & 0 \\ 0 & u & 1/\rho & 0 \\ 0 & \rho c^2 & u & 0 \\ 0 & \rho h & 0 & u \end{pmatrix} \quad (\text{A4})$$

with eigenvalues  $\lambda^{(-)} = u - c$ ,  $\lambda^{(o)} = u$ ,  $\lambda^{(e)} = u$ , and  $\lambda^{(+)} = u + c$ . We denote the second instance of the  $u$  eigenvalue with the superscript  $e$ , and its associated eigenvector only appears when the primitive variable system is augmented with  $\rho e$ .

Expressing the eigenvectors as a matrix,  $R = (r^{(-)}|r^{(o)}|r^{(e)}|r^{(+)})$  and  $L = (l^{(-)}|l^{(o)}|l^{(e)}|l^{(+)})^\top$ , we have

$$R = \begin{pmatrix} 1 & 1 & 0 & 1 \\ -c/\rho & 0 & 0 & c/\rho \\ c^2 & 0 & 0 & c^2 \\ h & 0 & 1 & h \end{pmatrix} \quad L = \begin{pmatrix} 0 & -\rho/2c & 1/2c^2 & 0 \\ 1 & 0 & -1/c^2 & 0 \\ 0 & 0 & -h/c^2 & 1 \\ 0 & \rho/2c & 1/2c^2 & 0 \end{pmatrix} \quad (\text{A5})$$

The derivation of these follows from  $Ar^{(\nu)} = \lambda^{(\nu)}r^{(\nu)}$  and  $l^{(\nu)}A = \lambda^{(\nu)}l^{(\nu)}$ , with  $l^{(i)} \cdot r^{(j)} = \delta_{ij}$ . Note that since the  $u$  eigenvalue is degenerate,  $\Delta q_s^{(o)} = \Delta q_s^{(e)}$ .

We can now write out the form of the interface states takes by simply multiplying out the dot products and doing the sum. We introduce the following notation (based on CW):

$$\beta_s^{(-)} \equiv (l^{(-)} \cdot \Delta q_s^{(-)}) = \frac{\rho}{2c} \left( -\Delta u_s^{(-)} + \frac{\Delta p_s^{(-)}}{\rho c} \right) \quad (\text{A6a})$$

$$\beta_s^{(o)} \equiv (l^{(o)} \cdot \Delta q_s^{(o)}) = \Delta \rho_s^{(o)} - \frac{\Delta p_s^{(o)}}{c^2} \quad (\text{A6b})$$

$$\beta_s^{(e)} \equiv (l^{(e)} \cdot \Delta q_s^{(e)}) = -\frac{h \Delta p_s^{(o)}}{c^2} + \Delta(\rho e)_s^{(o)} \quad (\text{A6c})$$

$$\beta_s^{(+)} \equiv (l^{(+)} \cdot \Delta q_s^{(+)}) = \frac{\rho}{2c} \left( \Delta u_s^{(+)} + \frac{\Delta p_s^{(+)}}{\rho c} \right) \quad (\text{A6d})$$

For these  $\beta$ 's and those that follow in the other sections, if the respective wave is not moving toward the interface, then the associated  $\beta_s^{(\nu)}$  is set to 0. With these definitions, and Eq. A1, we have

$$\rho_s = \tilde{\rho} - (\beta_s^{(-)} + \beta_s^{(o)} + \beta_s^{(+)}) \quad (\text{A7a})$$

$$u_s = \tilde{u} - \left( -\frac{c}{\rho} \beta_s^{(-)} + \frac{c}{\rho} \beta_s^{(+)} \right) \quad (\text{A7b})$$

$$p_s = \tilde{p} - (c^2 \beta_s^{(-)} + c^2 \beta_s^{(+)}) \quad (\text{A7c})$$

$$(\rho e)_s = \widetilde{(\rho e)} - (h \beta_s^{(-)} + \beta_s^{(e)} + h \beta_s^{(+)}) \quad (\text{A7d})$$

## A.2. Specific volume in place of density

CW consider a system with  $\tau \equiv 1/\rho$  replacing  $\rho$  in the primitive variable system and do the characteristic tracing in terms of this. We will denote this system as  $\hat{q} = (\tau, u, p, e)^\top$ . Now Eq. 4a is modified by substituting  $\rho = \tau^{-1}$  and expanding:

$$\frac{\partial \tau}{\partial t} + u \frac{\partial \tau}{\partial x} - \tau \frac{\partial u}{\partial x} = 0 \quad (\text{A8})$$

And our system is

$$\dot{\hat{q}}_t + \mathring{A} \hat{q}_x = 0 \quad (\text{A9})$$

with

$$\mathring{A}(\hat{q}) = \begin{pmatrix} u & -\tau & 0 & 0 \\ 0 & u & \tau & 0 \\ 0 & c^2/\tau & u & 0 \\ 0 & p\tau & 0 & u \end{pmatrix} \quad (\text{A10})$$

This has the same characteristic polynomial,  $|\mathring{A} - \lambda I| = 0$  as  $A(q)$ , so the eigenvalues are unchanged. The matrices of eigenvectors are:

$$\mathring{R} = \begin{pmatrix} 1 & 1 & 0 & 1 \\ c/\tau & 0 & 0 & -c/\tau \\ -c^2/\tau^2 & 0 & 0 & -c^2/\tau^2 \\ -p & 0 & 1 & -p \end{pmatrix} \quad \mathring{L} = \begin{pmatrix} 0 & \tau/2c & -\tau^2/2c^2 & 0 \\ 1 & 0 & \tau^2/c^2 & 0 \\ 0 & 0 & -p\tau^2/c^2 & 1 \\ 0 & -\tau/2c & -\tau^2/2c^2 & 0 \end{pmatrix} \quad (\text{A11})$$

As above, we introduce the notation  $\mathring{\beta}^{(\nu)} \equiv (\mathring{l}^{(\nu)} \cdot \Delta \mathring{q}^{(\nu)})$ :

$$\mathring{\beta}_s^{(-)} \equiv (\mathring{l}^{(-)} \cdot \Delta \mathring{q}_s^{(-)}) = \frac{1}{2C} \left( \Delta u_s^{(-)} - \frac{\Delta p_s^{(-)}}{C} \right) \quad (\text{A12a})$$

$$\mathring{\beta}_s^{(o)} \equiv (\mathring{l}^{(o)} \cdot \Delta \mathring{q}_s^{(o)}) = \Delta \tau_s^{(o)} + \frac{\Delta p_s^{(o)}}{C^2} \quad (\text{A12b})$$

$$\mathring{\beta}_s^{(e)} \equiv (\mathring{l}^{(e)} \cdot \Delta \mathring{q}_s^{(e)}) = -\frac{p \Delta p_s^{(o)}}{C^2} + \Delta e_s^{(o)} \quad (\text{A12c})$$

$$\mathring{\beta}_s^{(+)} \equiv (\mathring{l}^{(+)} \cdot \Delta \mathring{q}_s^{(+)}) = \frac{1}{2C} \left( -\Delta u_s^{(+)} - \frac{\Delta p_s^{(+)}}{C} \right) \quad (\text{A12d})$$

These  $\beta$ 's (excluding the 'e' case) are identical to Eq. 3.7 in CW. Inserting into Eq. A1 gives:

$$\tau_s = \tilde{\tau}_s - \left( \mathring{\beta}_s^{(-)} + \mathring{\beta}_s^{(o)} + \mathring{\beta}_s^{(+)} \right) \quad (\text{A13a})$$

$$u_s = \tilde{u}_s - \left( C \mathring{\beta}_s^{(-)} - C \mathring{\beta}_s^{(+)} \right) \quad (\text{A13b})$$

$$p_s = \tilde{p}_s - \left( -C^2 \mathring{\beta}_s^{(-)} - C^2 \mathring{\beta}_s^{(+)} \right) \quad (\text{A13c})$$

$$e_s = \tilde{e}_s - \left( -p \mathring{\beta}_s^{(-)} + \mathring{\beta}_s^{(e)} - p \mathring{\beta}_s^{(+)} \right) \quad (\text{A13d})$$

If we express  $\tilde{\tau} = 1/\tilde{\rho}$  and  $\mathcal{I}_s^{(o)}(\tau) = 1/\mathcal{I}_s^{(o)}(\rho)$ , then Eqs. A13a to A13c are identical to CW Eq. 3.6, giving:

$$\rho_s = \left[ \frac{1}{\tilde{\rho}_s} - \left( \mathring{\beta}_s^{(-)} + \mathring{\beta}_s^{(o)} + \mathring{\beta}_s^{(+)} \right) \right]^{-1} \quad (\text{A14})$$

This substitution says that we do the parabolic reconstruction of  $\rho$ , but the characteristic projection with  $\tau$ . We note that in evaluating these expressions, CW use  $\tilde{C} = \sqrt{\Gamma_1 \tilde{\rho}}$  instead of  $C$  constructed from the time-level n data.

### A.3. Using $\gamma_e$

For a general equation of state, we can combine the ideas of CG and CW to predict  $\gamma_e$  on the interfaces by first reconstructing it as a parabola. This is in spirit of what the FLASH dimensionally-split PPM solver does, but as we'll show here, there is a correction term that is necessary to account for the jump in  $\gamma_e$  across all waves.

We consider the same system as CW, augmented with the evolution equation for  $\gamma_e$ . We'll consider the primitive variable system  $\check{q} = (\tau, u, p, \gamma_e)^\top$ . Using Eq. 7, our system can be written as:

$$\check{q}_t + \check{A}\check{q}_x = 0 \quad (\text{A15})$$

with

$$\check{A}(\check{q}) = \begin{pmatrix} u & -\tau & 0 & 0 \\ 0 & u & \tau & 0 \\ 0 & c^2/\tau & u & 0 \\ 0 & -\alpha & 0 & u \end{pmatrix} \quad (\text{A16})$$

where we write  $\alpha \equiv (\gamma_e - 1)(\gamma_e - \Gamma_1)$  for shorthand. We notice that the structure and elements of this matrix are identical to that of  $\check{A}(\check{q})$  with the change  $p\tau \rightarrow -\alpha$ . The eigenvectors are then easily computable and found as:

$$\check{R} = \begin{pmatrix} 1 & 1 & 0 & 1 \\ c/\tau & 0 & 0 & -c/\tau \\ -c^2/\tau^2 & 0 & 0 & -c^2/\tau^2 \\ \alpha/\tau & 0 & 1 & \alpha/\tau \end{pmatrix} \quad \check{L} = \begin{pmatrix} 0 & \tau/2c & -\tau^2/2c^2 & 0 \\ 1 & 0 & \tau^2/c^2 & 0 \\ 0 & 0 & \alpha\tau/c^2 & 1 \\ 0 & -\tau/2c & -\tau^2/2c^2 & 0 \end{pmatrix} \quad (\text{A17})$$

As above, we introduce the notation  $\check{\beta}^{(\nu)} \equiv (\check{l}^{(\nu)} \cdot \Delta\check{q}^{(\nu)})$ . Because of the similarities to the CW system derived above, we see that  $\check{\beta}_s^{(-)} = \check{\beta}_s^{(-)}$ ,  $\check{\beta}_s^{(o)} = \check{\beta}_s^{(o)}$ , and  $\check{\beta}_s^{(+)} = \check{\beta}_s^{(+)}$ , and

$$\check{\beta}_s^{(e)} \equiv (\check{l}^{(e)} \cdot \Delta\check{q}_s^{(e)}) = \frac{\alpha\Delta p_s^{(o)}}{\tau C^2} + \Delta\gamma_{e_s}^{(o)} \quad (\text{A18})$$

Considering only how the  $\gamma_e$  state appears in the characteristic tracing, we see:

$$\gamma_{e_s} = \tilde{\gamma}_{e_s} - \check{\beta}_s^{(-)}\frac{\alpha}{\tau} - \check{\beta}_s^{(e)} - \check{\beta}_s^{(+)}\frac{\alpha}{\tau} \quad (\text{A19})$$

and if we simplify things by taking the reference state,  $\tilde{\gamma}_{e_s}$  to be zero, then we find:

$$\gamma_{e_s} = \mathcal{I}_s^{(o)}(\gamma_e) + \alpha \left[ -\frac{\check{\beta}_s^{(-)}}{\tau} + \frac{\mathcal{I}_s^{(o)}(p)}{\tau C^2} - \frac{\check{\beta}_s^{(+)}}{\tau} \right] \quad (\text{A20})$$



We note that with a constant-gamma gas (like an ideal gas), then  $\mathcal{I}_s^{(\circ)}(\gamma_e) = \gamma_e$  and  $\alpha = 0$ , as expected. Written as above, we see that the  $\gamma_e$  interface state can be viewed as the average of  $\gamma_e$  under the reconstructed parabola over the region traced by the  $\lambda^{(\circ)} = u$  wave plus a correction term that is proportional to  $\alpha$ . In FLASH, to the best of our knowledge, only the first term is present in the dimensionally-split PPM solver.

## B. Exact Riemann Solution with a Degenerate Gas

To test the variations on the standard PPM method we need a test problem with an exact solution for the general stellar equation of state. CG (section 1) describe how to exactly solve the Riemann problem for a general equation of state. As with a gamma-law gas, across the left and right waves, different functions connect the left/right state to the star state, and the resulting equation for  $p_\star$  needs to be solved via an iterative procedure. However, unlike the gamma-law gas, one cannot write down a closed-form expression for either the rarefaction or shock cases. For the rarefaction, a system of ODEs must be integrated, while for the shock, a root-finding procedure operates on the Rankine-Hugoniot jump conditions.

Note that in the following, we assume a constant composition. Adding a composition jump at the interface is straightforward, as the composition will only change across the contact wave (this follows from the structure of the right eigenvectors). Below we summarize the solution procedure from CG, filling in some implementation details:

- *Initial guess:* We need an initial guess for  $p_\star$ . We use the two-shock approximation from Toro (1997), Eq. 9.42:

$$p_\star = [(W_r p_l + W_l p_r) + W_l W_r (u_l - u_r)] / (W_l + W_r) \quad (\text{B1})$$

with the initial guess for the wave speeds taken to be the Lagrangian sound speed,  $W_s = \sqrt{\Gamma_{1s} p_s \rho_s}$

- *$p_\star$  iteration loop:* We use perform the Newton iteration described in CG. For  $s = \{l, r\}$ , we apply the shock jump conditions if  $p_\star > p_s$ , and use the Riemann invariants for a rarefaction otherwise. In each case, our goal is to find  $Z_s \equiv |dp_\star/du_{x,s}|$  and  $W_s$ .

- *Shock solution:* For a shock, we solve the Rankine-Hugoniot jump conditions. This takes the form (see CG Eq. 12):

$$f(W_s) = W_s^2 \left\{ e \left( p_\star, \left[ \frac{1}{\rho_s} - \frac{p_\star - p_s}{W_s^2} \right]^{-1} \right) - e_s \right\} - \frac{1}{2}(p_\star^2 - p_s^2) \quad (\text{B2})$$

with the solution corresponding to  $f(W_s) = 0$ . Here, we used the mass Rankine-Hugoniot condition to express the density in the EOS function in terms of  $p_*$  and  $W_s$ :

$$\rho_* = \left[ \frac{1}{\rho_s} - \frac{p_* - p_s}{W_s^2} \right]^{-1} \quad (\text{B3})$$

We solve this via Newton iteration, using the derivative:

$$f'(W_s) = 2W_s \{e(p_*, \rho_*) - e_s\} - \frac{2}{W_s} \frac{\partial e}{\partial \rho} \Big|_p (p_* - p_s) \rho_*^2 \quad (\text{B4})$$

We iterate until  $|f/f'| < \epsilon W_s$ , where  $\epsilon$  is a small tolerance. We evaluate that thermodynamic derivative by expressing our EOS as  $e(\rho, T(\rho, p))$ :

$$\frac{\partial e}{\partial \rho} \Big|_p = \frac{\partial e}{\partial \rho} \Big|_T + \frac{\partial e}{\partial T} \Big|_p \frac{\partial T}{\partial \rho} \Big|_p = \frac{\partial e}{\partial \rho} \Big|_T - \frac{\partial e}{\partial T} \Big|_p \frac{\partial p}{\partial \rho} \Big|_T \left( \frac{\partial p}{\partial T} \Big|_\rho \right)^{-1} \quad (\text{B5})$$

where we used the constancy of pressure as:  $dp = (\partial p/\partial \rho)|_T d\rho + (\partial p/\partial T)|_\rho dT = 0$  to eliminate  $\partial T/\partial \rho|_p$ .

Once we find  $W_s$ , we can evaluate  $Z_s$  using CG Eqs. 20 and 23. Two more thermodynamic derivatives are needed:

$$\frac{\partial p}{\partial e} \Big|_\rho = \frac{\partial p}{\partial T} \Big|_\rho \left( \frac{\partial e}{\partial T} \Big|_\rho \right)^{-1} \quad (\text{B6})$$

$$\frac{\partial p}{\partial \rho} \Big|_e = \frac{\partial p}{\partial \rho} \Big|_T - \frac{\partial e}{\partial \rho} \Big|_T \left( \frac{\partial e}{\partial T} \Big|_\rho \right)^{-1} \quad (\text{B7})$$

and in terms of specific volume,  $\tau \equiv 1/\rho$ ,

$$\frac{\partial p}{\partial \tau} \Big|_T = -\rho^2 \frac{\partial p}{\partial \rho} \Big|_T \quad (\text{B8})$$

These can be derived in a similar fashion as shown above.

We use the approximation for  $W_s$  in the case where we know  $\gamma_*$  (CG, Eq. 24) as the initial guess for  $W_s$ . We estimate a value for  $\gamma_*$  from the evolution equation CG derive, CG Eq. 31.

- *Rarefaction solution:* In the case of a rarefaction, we simply integrate the Riemann invariant ODEs. We integrate:

$$\frac{d\tau}{dp} = \begin{cases} -C^{-2} & \text{left rarefaction} \\ -C^{-2} & \text{right rarefaction} \end{cases} \quad \frac{du}{dp} = \begin{cases} -C^{-1} & \text{left rarefaction} \\ C^{-1} & \text{right rarefaction} \end{cases} \quad (\text{B9})$$

Here  $C = C(\tau, p)$  is the Lagrangian sound speed. The integration is done simply with 4-th order Runge Kutta from  $p = p_s$  to  $p_*$ . Then  $W_s = C$  and  $Z_s$  is given by CG Eq. 16.

- *Sampling the solution:*

Once we have solved for the wave structure, we can sample the solution at a given time,  $t$ . Given  $N$  points, the coordinate centers are  $x_i = (i + 1/2)\Delta x$  for  $i = 1, \dots, N$ , with  $\Delta x = (x_{\max} - x_{\min})/N$ . Then we define

$$\xi_i = \frac{x_i - \frac{1}{2}(x_{\max} - x_{\min})}{t} \tag{B10}$$

The speed of the contact  $u_*$  tells us which states we need to deal with, and the evaluation of the solution proceeds from CG Eq. 15 and following.

The only complication is the case where we are sampling inside the rarefaction. As suggested in CG, we integrate the Riemann invariants, however, we found that it is easiest to rewrite them with  $u$  as the independent variable. We integrate:

$$\frac{d\tau}{du} = \begin{cases} C^{-1} & \text{left rarefaction} \\ -C^{-1} & \text{right rarefaction} \end{cases} \quad \frac{dp}{du} = \begin{cases} -C & \text{left rarefaction} \\ C & \text{right rarefaction} \end{cases} \tag{B11}$$

We integrate from  $u = u_s$  to

$$u_{\text{stop}} = \begin{cases} \xi + c(\tau, p) & \text{left rarefaction} \\ \xi - c(\tau, p) & \text{right rarefaction} \end{cases} \tag{B12}$$

We don't know  $u_{\text{stop}}$  at the start of the integration (since  $c$  depends on the state), so we evaluate it each step. Again we use Runge-Kutta integration, and we adjust our stepsize to stop at the converged  $u_{\text{stop}}$ .

We use this solution to generate several exact shock tube profiles to compare with the PPM solutions. It is easier to specify the initial conditions in terms of a jump in  $(\rho, u, T)$  instead of  $(\rho, u, p)$  and then compute the pressure via the equation of state. Additionally, for this equation of state, we need to specify the composition of the gas—we take it to be pure  $^{12}\text{C}$ .

Since even different versions of the same equation of state can have slightly different thermodynamics, we do not provide a table of the solution output for the problems listed here. Instead, the complete source code for this exact solver is available in the CASTRO source distribution (in the `Util/exact_riemann/` subdirectory). This can be built with

either the general stellar equation of state (Timmes & Swesty 2000) or a gamma-law EOS. All the necessary inputs files for the tests described here are provided.

We devise 4 tests. The first 3 are analogous to tests 1 through 3 in Toro (1997): test 1 is a Sod-like problem, test 2 is a double rarefaction, and test 3 is a strong shock. The last test, test 4, mimics the conditions present at the edge of a star when it is not very well resolved on a grid—a common issue with multi-dimensional stellar simulations. Table 1 lists all the parameters, including the length of the domain,  $L$ , and the end time of the simulation,  $t$ . All tests used outflow (zero-gradient) boundary conditions. For test 4, because of the large drop in density, the Coulomb corrections in the equation of state were disabled to avoid unphysical regions in the thermodynamic space.

## REFERENCES

- Almgren, A. S., Bell, J. B., Rendleman, C. A., & Zingale, M. 2006, *ApJ*, 637, 922
- Almgren, A. S., et al. 2010, *ApJ*, 715, 1221, 1005.0114
- Bell, J. B., Colella, P., & Trangenstein, J. A. 1989, *Journal of Computational Physics*, 82, 362
- Bryan, G. L., et al. 2014, *ApJS*, 211, 19, 1307.2265
- Colella, P. 1990, *Journal of Computational Physics*, 87, 171
- Colella, P., & Glaz, H. M. 1985, *Journal of Computational Physics*, 59, 264
- Colella, P., Glaz, H. M., & Ferguson, R. E. 1997, unpublished manuscript
- Colella, P., & Sekora, M. D. 2008, *Journal of Computational Physics*, 227, 7069
- Colella, P., & Woodward, P. R. 1984, *Journal of Computational Physics*, 54, 174
- Einfeldt, B. 1988, *SIAM J Numer Anal*, 25, 294
- Fryxell, B., Müller, E., & Arnett, D. 1989, Max-Planck-Institut für Astrophysik Report 449
- Fryxell, B., et al. 2000, *ApJS*, 131, 273
- Harten, A., Lax, P. D., & van Leer, B. 1983, *SIAM Rev*, 25, 35
- McCorquodale, P., & Colella, P. 2011, *Comm Appl Math and Comput Sci*, 6, 1
- Miller, G. H., & Colella, P. 2002, *Journal of Computational Physics*, 183, 26
- Sod, G. A. 1978, *Journal of Computational Physics*, 27, 1
- Stone, J. M., Gardiner, T. A., Teuben, P., Hawley, J. F., & Simon, J. B. 2008, *ApJS*, 178, 137, 0804.0402
- Timmes, F. X., & Swesty, F. D. 2000, *ApJS*, 126, 501
- Toro, E. F. 1997, *Riemann Solvers and Numerical Methods for Fluid Dynamics* (Springer)

Table 1. Test problems.

quantity	test 1		test 2		test 3		test 4	
	left	right	left	right	left	right	left	right
$\rho$ (g cm <sup>-3</sup> )	10 <sup>7</sup>	10 <sup>6</sup>	10 <sup>7</sup>	10 <sup>7</sup>	10 <sup>6</sup>	10 <sup>6</sup>	10 <sup>2</sup>	10 <sup>-4</sup>
$T$ (K)	10 <sup>8</sup>	10 <sup>6</sup>	10 <sup>8</sup>	10 <sup>8</sup>	10 <sup>9</sup>	10 <sup>6</sup>	10 <sup>7</sup>	10 <sup>7</sup>
$u$ (cm/s)	0	0	-10 <sup>8</sup>	10 <sup>8</sup>	0	0	0	0
$L$ (cm)	10 <sup>6</sup>		10 <sup>5</sup>		2 × 10 <sup>5</sup>		10 <sup>5</sup>	
$t$ (s)	8 × 10 <sup>-4</sup>		8 × 10 <sup>-5</sup>		2 × 10 <sup>-4</sup>		3 × 10 <sup>-4</sup>	

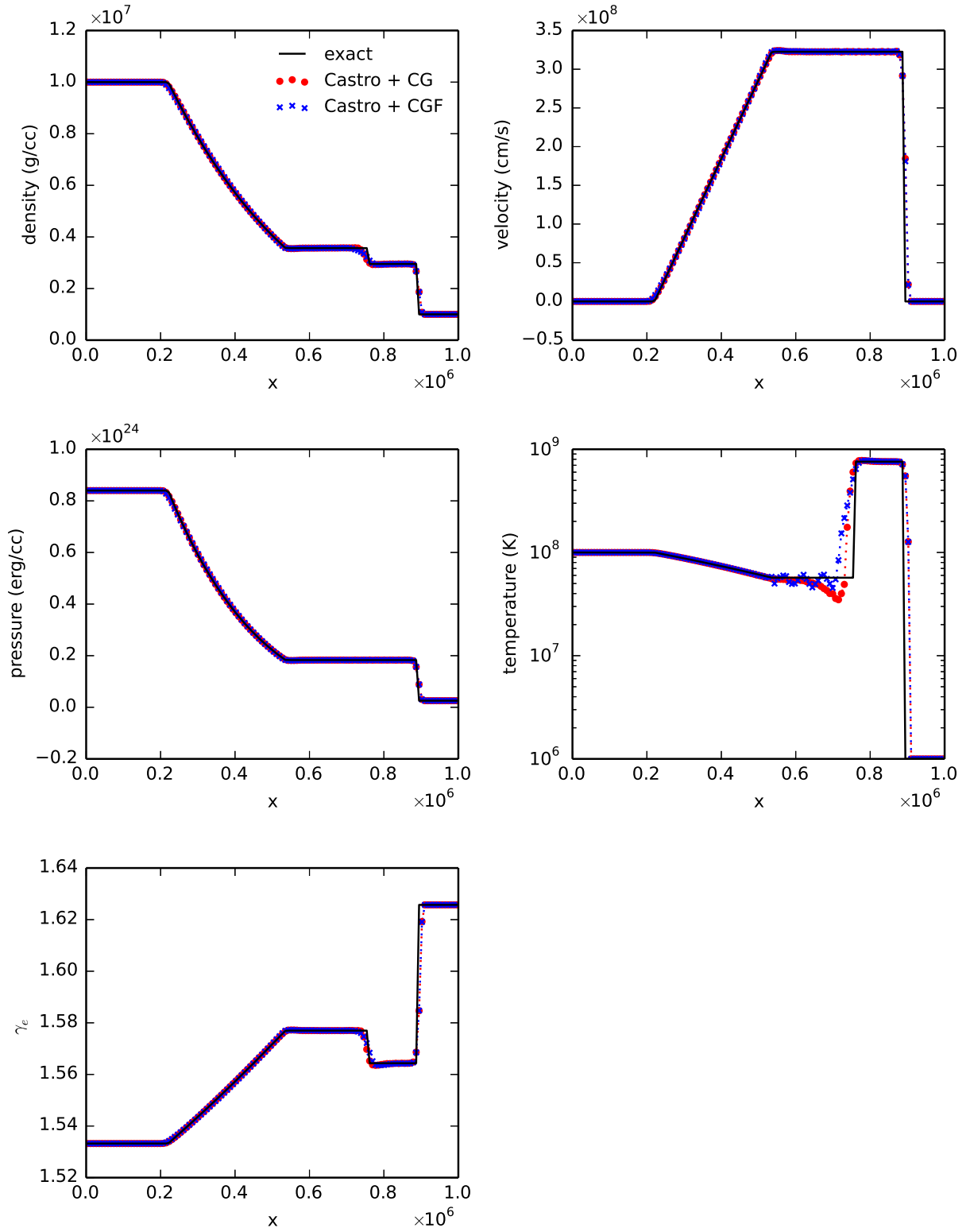


Fig. 3.— Sod-like test 1 problem with the general EOS comparing the differences between the CG and CGF Riemann solvers

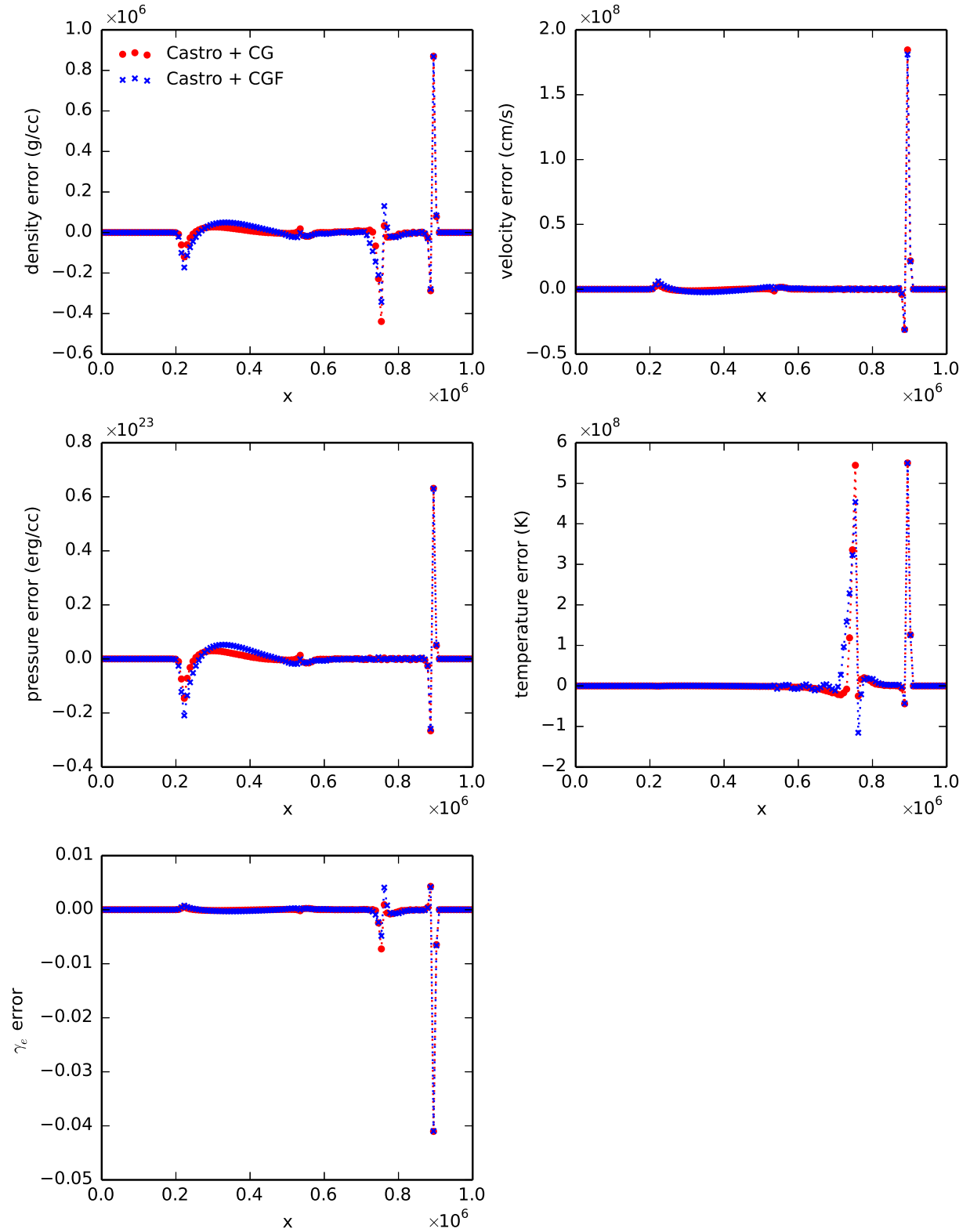


Fig. 4.— Errors in the Sod-like test 1 problem with the general EOS comparing the differences between the CG and CGF Riemann solvers



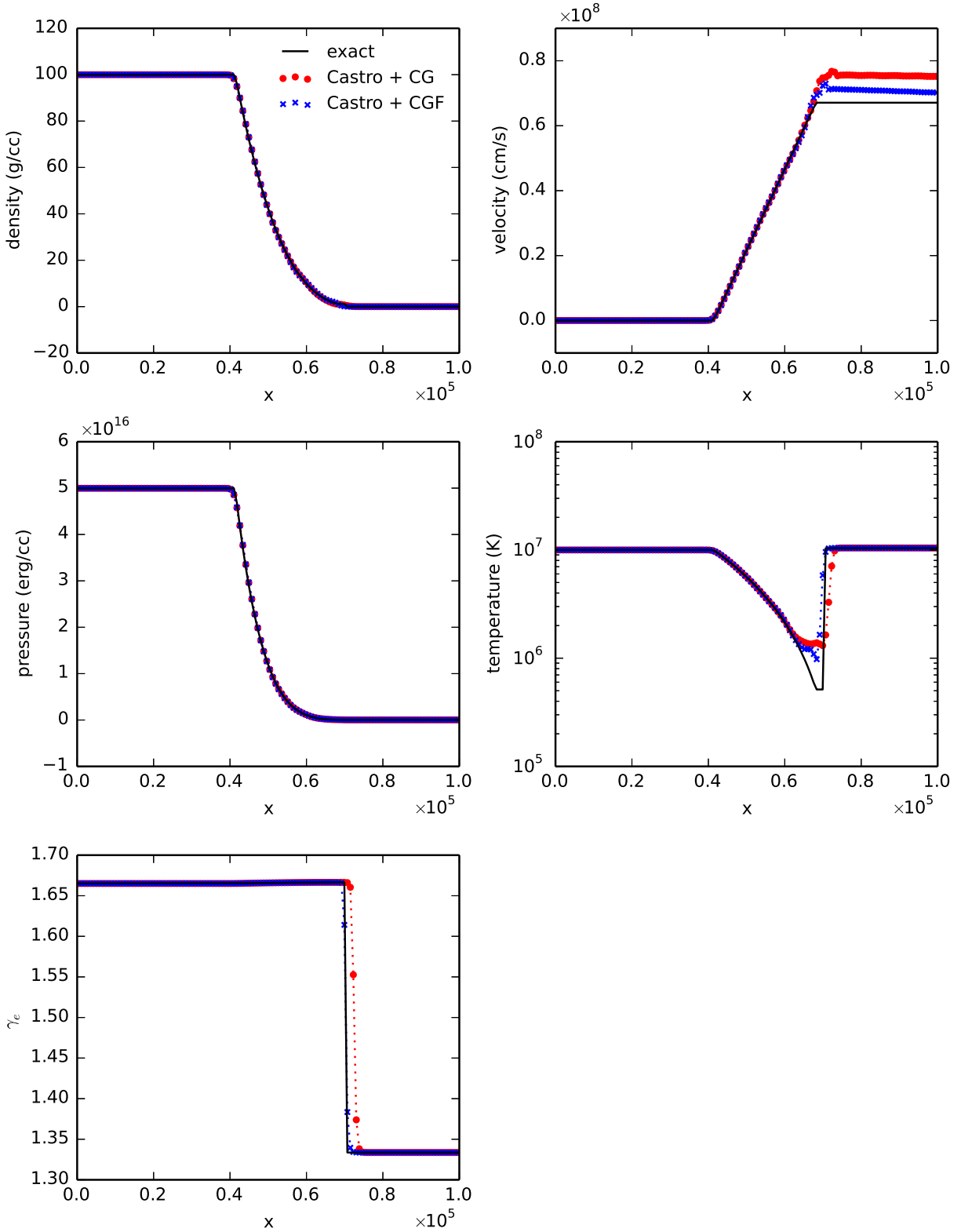


Fig. 5.— Solutions for the “stellar edge” test 4 problem with the general EOS comparing the differences between the CG and CGF Riemann solvers

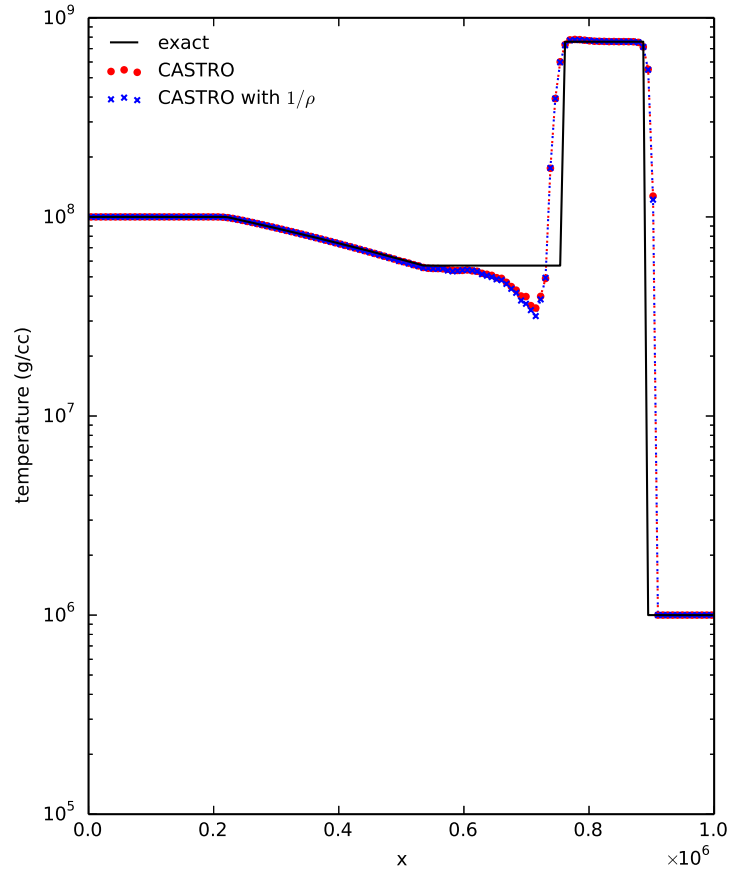


Fig. 6.— Sod-like test 1 problem with the general EOS comparing the use of  $\tau = 1/\rho$  (CW) to  $\rho$  (MC) in the characteristic tracing. Only the temperature is shown

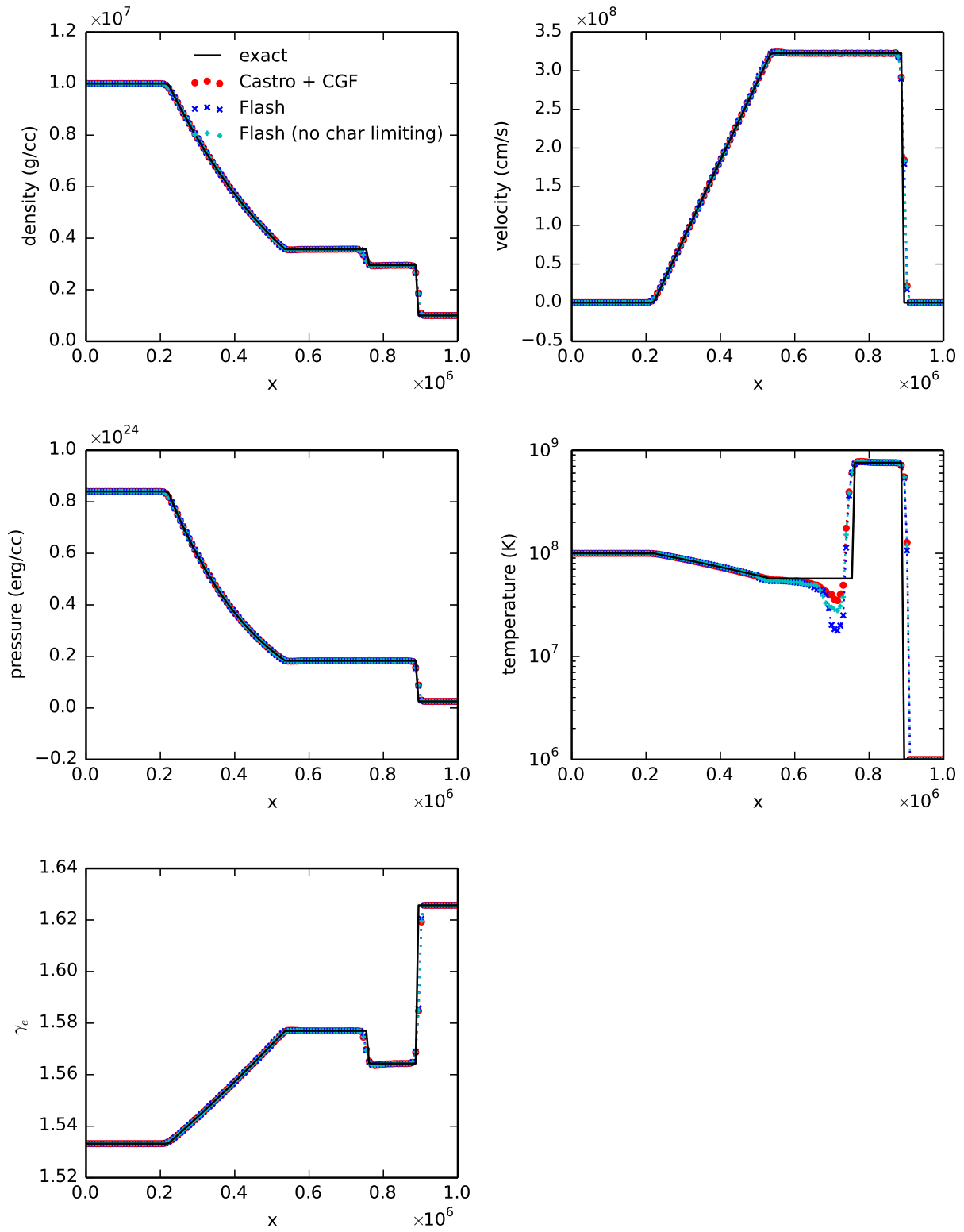


Fig. 7.— A comparison of CASTRO to FLASH for test 1.

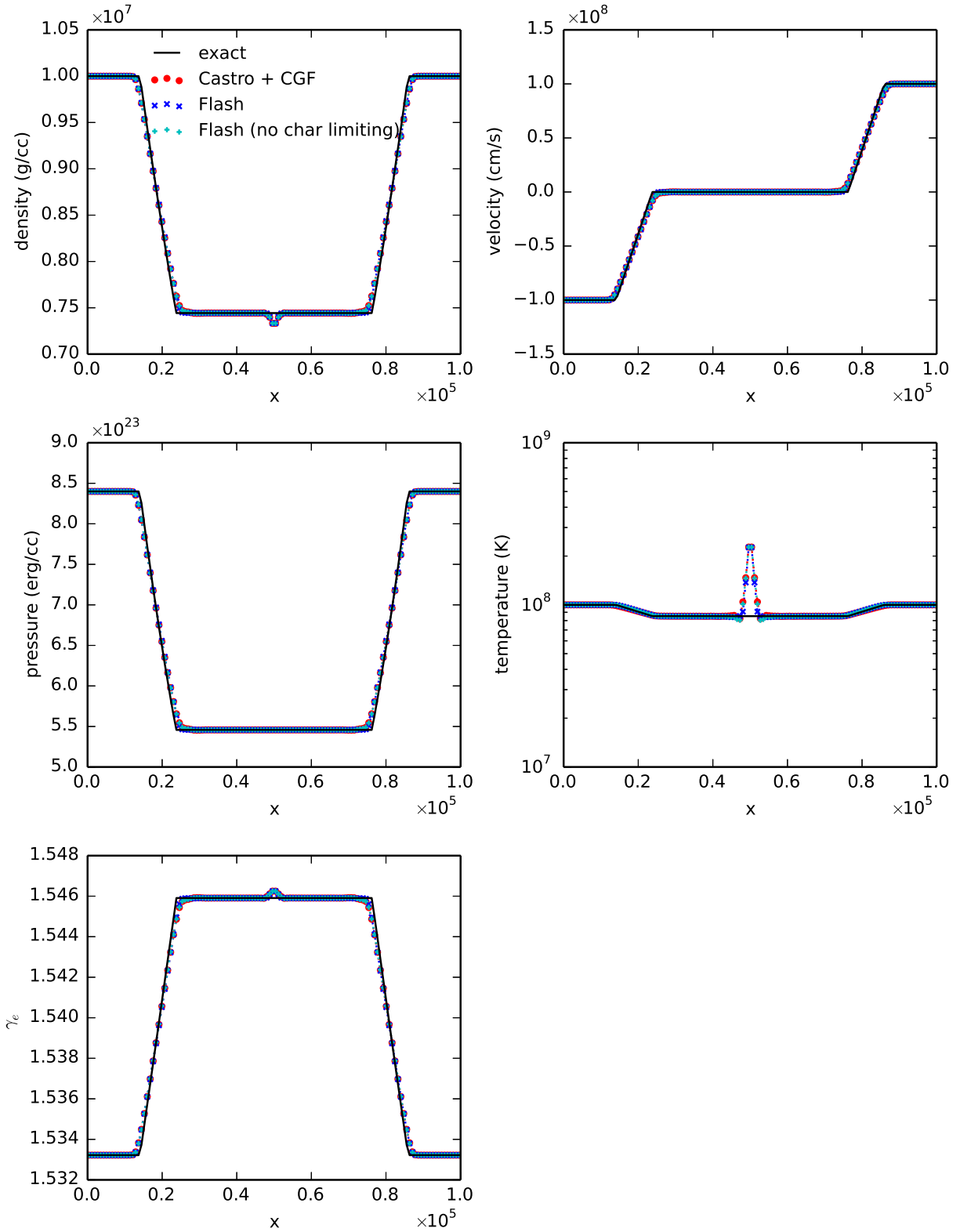


Fig. 8.— A comparison of CASTRO to FLASH for test 2.

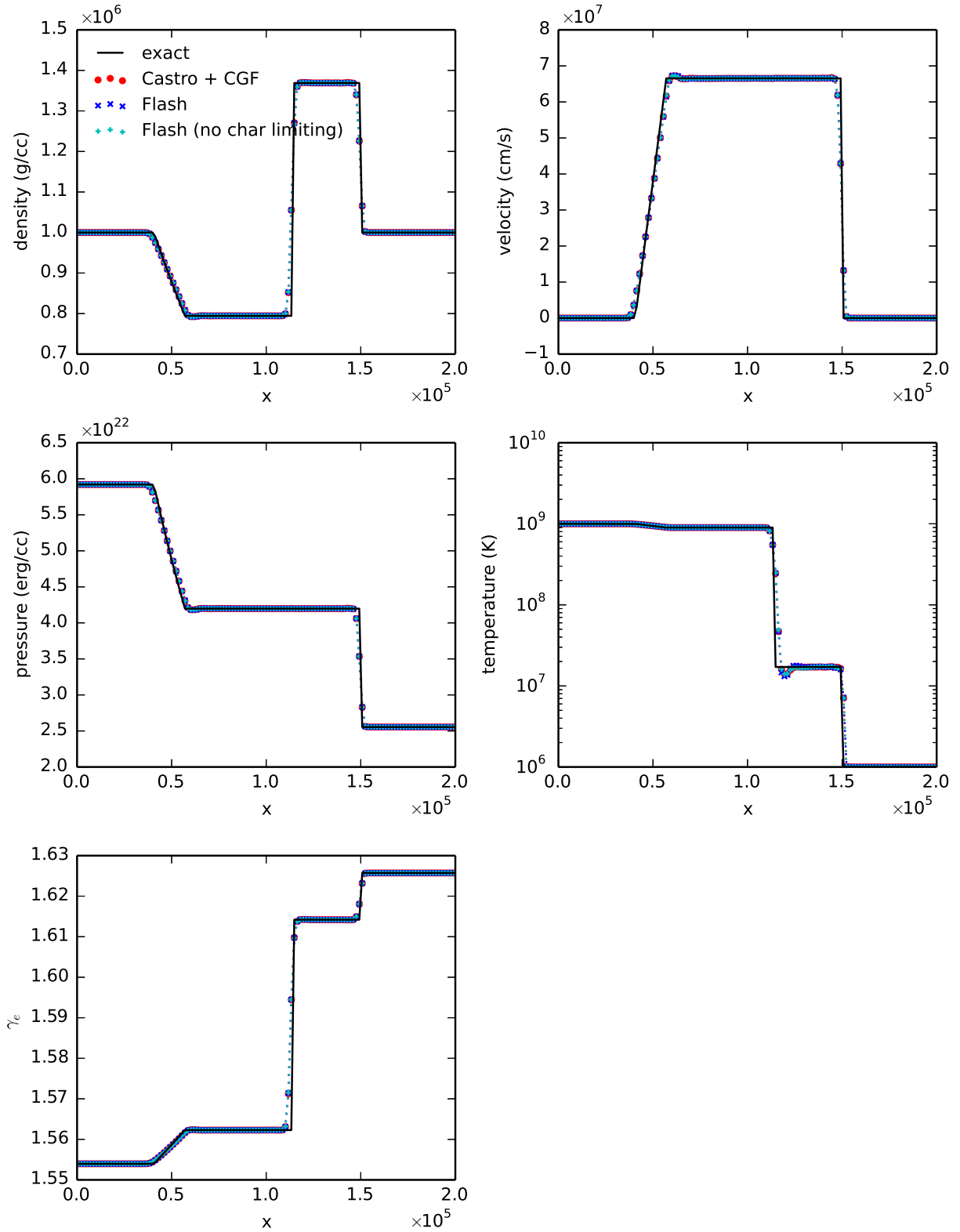


Fig. 9.— A comparison of CASTRO to FLASH to test 3.

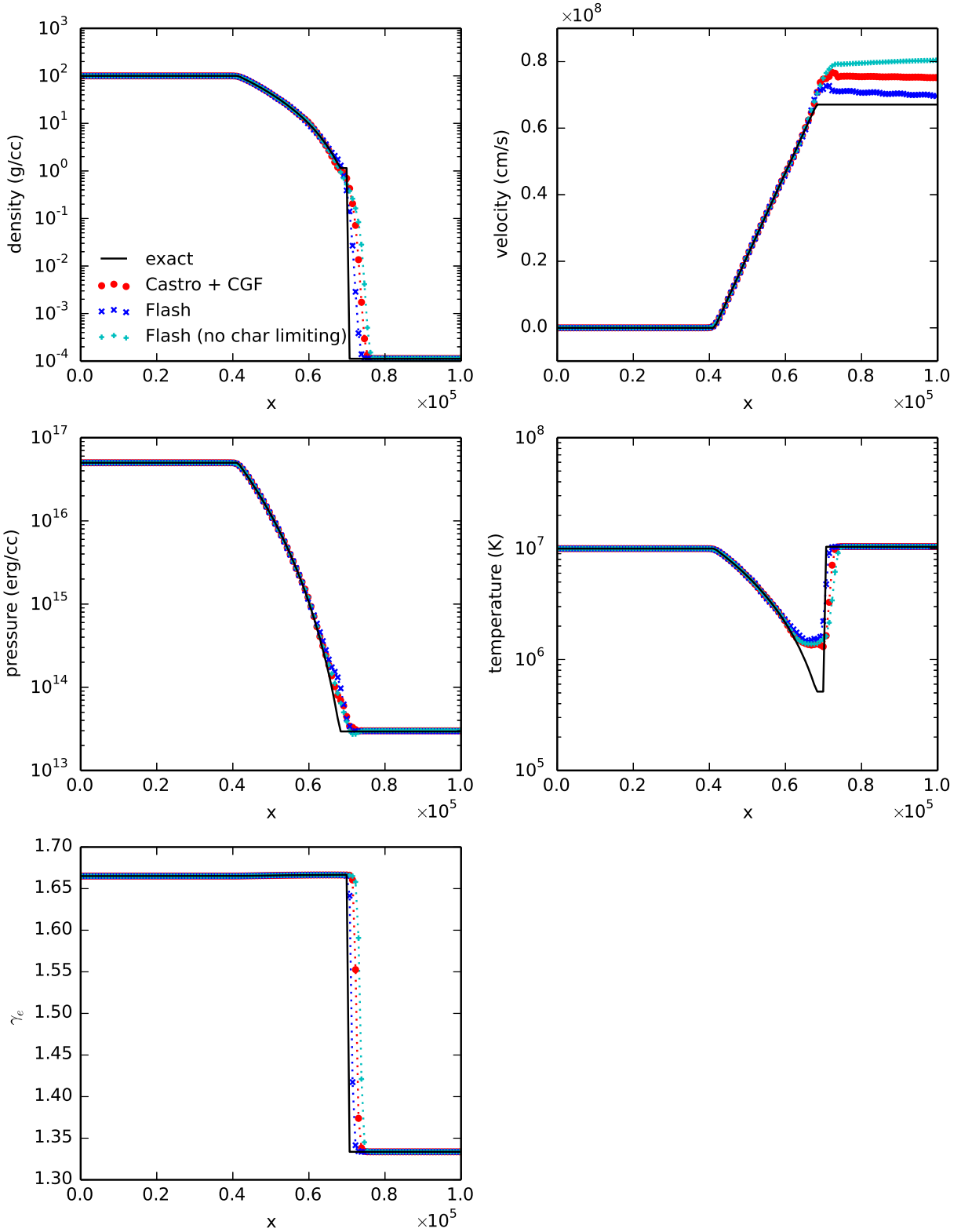


Fig. 10.— A comparison of CASTRO to FLASH to test 4.